PETROGRAPHIC SETTING OF BADDELEYITE IN ENRICHED BASALTIC SHERGOTTITES

A. I. Sheen, C.D.K. Herd

Department of Earth and Atmospheric Sciences, 1-26 Earth Sciences Building, University of Alberta, Edmonton, Alberta, Canada, T6G 2E3. (asheen@ualberta.ca)

INTRODUCTION

- High-resolution *in-situ* secondary ion mass spectrometry (SIMS) has enabled successful U–Pb baddeleyite (ZrO_2) geochronology of shergottites [1, 2]
- In shergottites, baddeleyite crystallized from fractionated portions of the magma together with other late-stage phases (Fe-rich cpx, Fe-Ti oxides, Ca-phosphates, fayalite, glass); crystallization is controlled by geochemistry and petrography [3]
- Amenability to U–Pb baddeleyite age dating depends on size and abundance of baddeleyite grains in the sample
- Baddeleyite searching in shergottites is generally done via SEM and EPMA methods; smaller grains require higher detection resolution

Martian meteorite are currently the only readily available samples of Mars and the primary source of absolute chronology of the planet. Compared to traditional mineral dissolution methods, *in-situ* SIMS geochronology preserves petrographic context. Growing interest in SIMS U–Pb baddeleyite analysis is fueled by upcoming Mars sample return missions. Since baddeleyite distribution in Martian meteorites varies [3], it is crucial to establish proxies for assessing whether a sample contains enough baddeleyite grains of sufficient size to enable SIMS U–Pb geochronology. To achieve this, we examined eight undated basaltic shergottites using a combination of methods to find and characterize baddeleyite occurrences.

METHODS

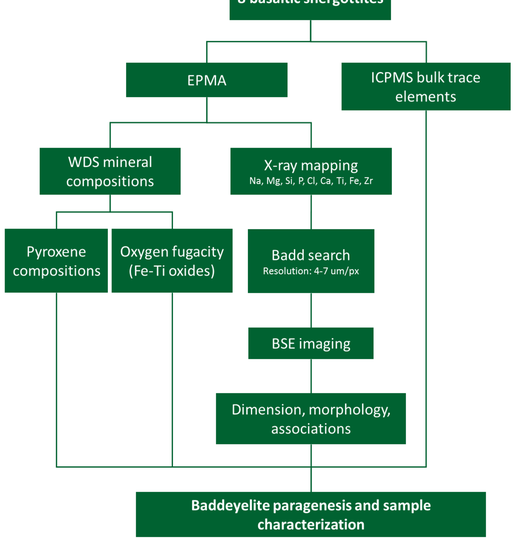

RESULTS

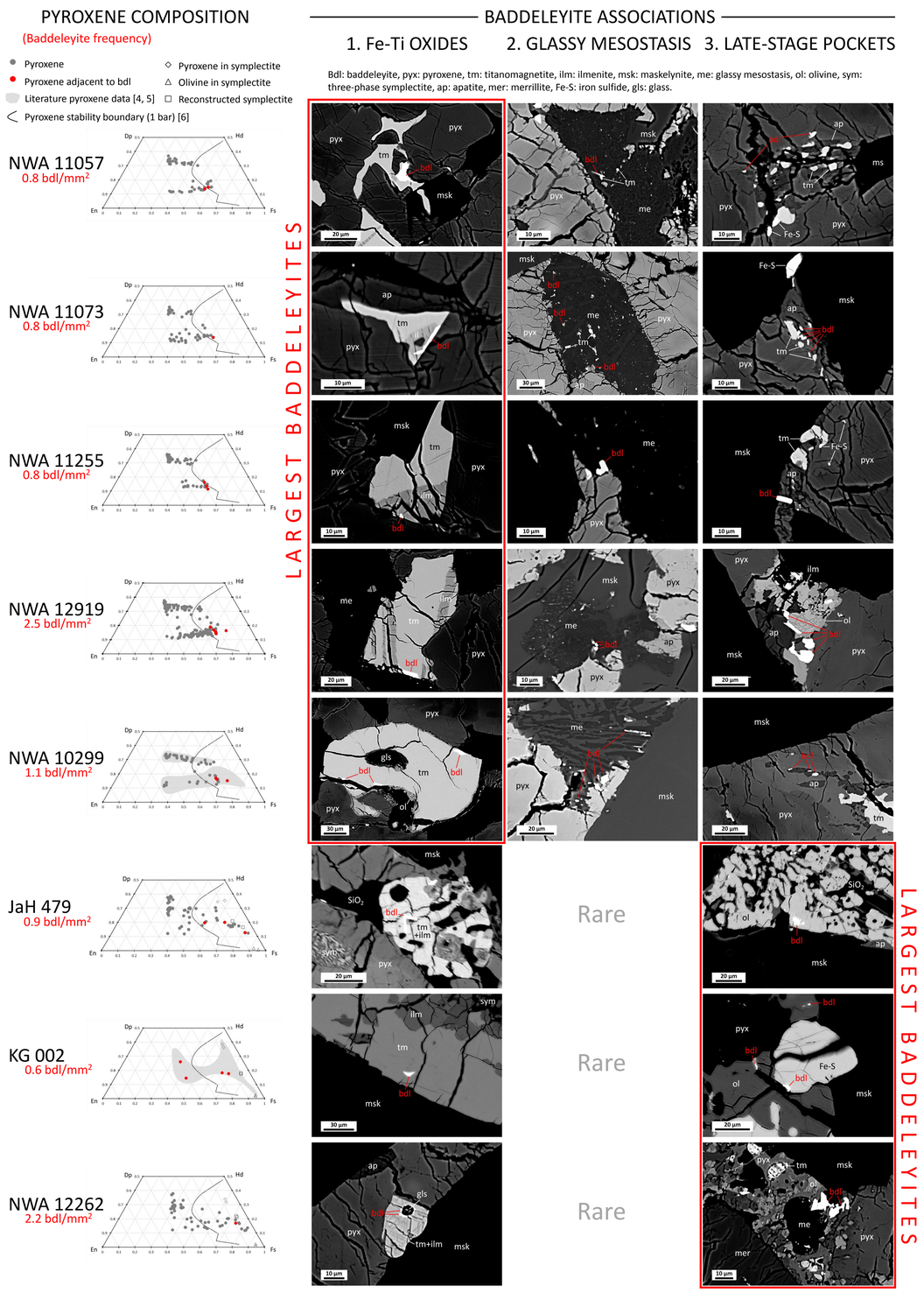

CONTROLS ON BADDELEYITE CRYSTALLIZATION

1. Bulk Zr budget in parent melt

Zirconium behaves as an incompatible trace element in shergottite magmas, becoming more enriched in the melt during crystallization. Hence baddeleyite occurrence should depend on bulk Zr content of the shergottite parent melt, to the first order [3].

While bulk Zr data are not available for all of the studied samples, there is generally a positive correlation between baddeleyite frequency and bulk concentration of incompatible elements (e.g., P, REE; see Figure). This demonstrates that baddeleyite is more likely to be found in samples that are more enriched in incompatible elements.

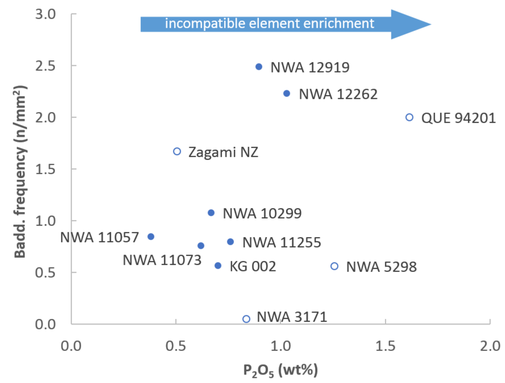

Baddeleyite frequency (expressed as number of grains per mm^2) vs P_2O_5 for the studied samples (solid circles), along with samples reported in [3] (open circles). P_2O_5 data sources: Zagami [9], QUE 94201 [10], NWA 3171, 5298 [11].

2. Degree of fractional crystallization

Fractional crystallization causes a melt to be progressively enriched in Fe. This is recorded in increasing ferroan content (expressed as Fs endmember) in pyroxene from cores to rims. Baddeleyite in samples with pyroxenes plotting below ~$Fs_{70–80}$ (e.g., NWA 11057) is generally less abundant than in samples with pyroxenes extending beyond Fs_{90} (e.g., NWA 12262). This indicates that melts which have undergone protracted fractionation will be more enriched in incompatible elements, favoring baddeleyite crystallization; similar trends were observed by [3].

Pyroxene compositions above ~Fs_{70} also indicate metastable crystallization from extensively fractionated melts. This is consistent with the presence of symplectite (as breakdown product of pyroxferroite/metastable pyroxene, [12]) and the occurrence of baddeleyite in silica-bearing assemblages (e.g, NWA 12662; [1]).

3. Distribution of Zr in late-stage assemblages

Samples with a high- and low-Ca pyroxene (Zagami-like) compositional trend contain the largest baddeleyite grains in Fe-Ti oxides. In samples without such a trend and where pyroxene compositions extend beyond the 1-bar stability boundary, the largest baddeleyite grains occur in coarse, silica-bearing mesostasis. This suggests that baddeleyite in the former group of samples is stable earlier in the crystallization sequence.

It has been noted that Zr becomes more compatible in Fe-Ti oxides at lower oxygen fugacity (fO_2), causing baddeleyite to crystallize preferentially in mesostasis after Fe-Ti oxide crystallization [3]. The majority of the studied samples have a narrow fO_2 range of -1.5 to -1.0 ΔQFM and do not clearly distinguish between samples with different predominant styles of baddeleyite association. NWA 12262 has higher fO_2 value of +0.1 ΔQFM as well as the highest baddeleyite frequency among the studied samples. However baddeleyite in NWA 12262 mostly occurs in coarse late-stage pockets, similar to other samples with high pyroxene ferroan content (JaH 479, KG 002). Hence fractional crystallization appears to have greater control on the style of baddeleyite associations. The higher fO_2 value of NWA 12262 is interpreted to reflect the more fractionated composition of the bulk rock, which favors baddeleyite crystallization.

BADDELEYITE ASSOCIATIONS

Three main occurrence types were found:

1. Inclusions within or on the edge of Fe-Ti oxides (Fe-Ti OXIDES)

2. Within fine-grained pockets of glassy mesostasis containing intergrown K-feldspar and glass, often with Fe-Ti oxides, chlorapatite, and Fe-rich pyroxene (GLASSY MESOSTASIS)

3. Within coarse-grained late-stage pockets containing Fe-rich pyroxene ± Ca-phosphates ± Fe-sulfides ± fayalitic olivine ± Fe-Ti oxides ± silica (LATE-STAGE POCKETS)

Less commonly, baddeleyite occurs on the margins of large grains of late-crystallizing minerals such as merrilite and ferroan pyroxene. Regardless of the occurrence, pyroxene and olivine adjacent to baddeleyite generally have the most ferroan compositions in the sample.

Table 1. Baddeleyite grain frequency and dimension statistics determined through EPMA mapping.

Sample	Frequency (n/mm²)	Avg. Grain Length (µm)	σ	Max. Grain Length (µm)	Avg. l:w Ratio	n	Pyroxene Fs Endmember (%)*	Oxygen Fugacity (logΔQFM)	σ	$La/Yb_{(N)}$**
NWA 11057	0.8	3.3	3.2	7	2.3	36	22-60	-1.4	0.2	0.87
NWA 11073	0.8	2.7	1.9	9	2.4	30	24-61	-1.5	0.2	0.88
NWA 11255	0.8	3.0	2.1	8	2.6	34	22-59	-1.1	0.1	0.93
NWA 12919	2.5	2.5	2.4	14	3.3	106	19-68	-1.1	0.2	0.87
NWA 10299	1.1	5.0	2.8	10	2.4	76	22-81	-1.4	0.5	0.94
JaH 479	0.9	6.7	1.5	24	2.8	97	21-83	-1.2	0.3	0.75
KG 002	0.6	3.0	1.9	9	2.5	60	26-96	-1.0	0.2	0.85
NWA 12262	2.2	3.2	2.3	10	2.1	79	24-83	+0.1	0.1	1.03

* Pyroxene data sources: KG 002 [4], NWA 10299 [5]; remaining values are from this study. ** Bulk rock, normalized to CI values. Data sources: JaH 479 [7], KG 002 [4], NWA 11073 and 11255 [8].

IMPLICATIONS & FUTURE WORK

- Baddeleyite crystallization in basaltic shergottites is controlled by the combination of incompatible element content in the parent melt, the degree of fractional crystallization, and the distribution of Zr among major phases and late-stage assemblages
- Among the studied samples, those with higher incompatible element content and with pyroxene compositions trending closer towards the Fs-Hd join generally display a higher abundance of baddeleyite grains
- The largest baddeleyite grains tend to have specific petrographic associations depending on pyroxene composition trends. This may be instrumental for predicting where sizable grains suitable for SIMS analysis can be found in an unknown sample
- Our approach can be applied towards assessment of other basaltic shergottite samples for U–Pb baddeleyite analysis feasibility, especially where only preliminary compositional data are available
- Next steps: CL and EBSD imaging of selected baddeleyite grains to assess microstructural and chemical features. This will address the following questions: Have these grains been subjected to shock modification? Which grains are more likely to yield undisturbed igneous U–Pb signatures?

ACKNOWLEDGEMENTS

Samples for this study were provided by Tony Irving (NWA 11057, 11073, 11255, 12266) and Julia Roszjar (KG 002). Analytical assistance was provided by Andrew Locock (EPMA) and Guangcheng Chen (ICP-MS). Funding by NSERC Grant RGPIN-2018-04902 to CDKH and NSERC CGS-D to AIS.

REFERENCES

[1] Moser D.E. et al. (2013) Nature, 499, 454-458. [2] Zhou Q. et al. (2013) EPSL, 374, 156-163. [3] Herd C.D. et al. (2018) AGU Monograph, 137-166. [4] Llorca J. et al. (2013) Meteorit. Planet. Sci., 48, 493-513. [5] Jean M.M. et al. (2016) LPS XLVII, Abstract #2698. [6] Lindsley D.H. (1983) Am. Mineral., 68, 477-493. [7] Lorenz C.A. et al. (2010) Meteorit. Planet. Sci., 45, A121. [8] Lapen T.J. et al. (2018) LPS XLIX, Abstract #2773. [9] Lodders et al. (1998) Meteorit. Planet. Sci., 33, A183-A190. [10] Kring et al. (2003) Meteorit. Planet. Sci., 38, 1833-1848. [11] Day et al. (2018) Nat. Commun., 9, 4799. [12] Aramovich C.J. et al. (2002) Am. Mineral., 87, 1351-1359.